

TUTDoR

Correlator-based multipath detection technique for a global positioning system/ GNSS receiver.

Item Type	Article
Authors	Amani, Elie;Djouani, Karim;De Boer, Jean-Rémi;Kurien, Anish;Vigneau, Willy
DOI	http://dx.doi.org/10.1049/iet-rsn.2017.0379
Publisher	Wiley Institution of Engineering and Technology (IET)
Rights	Attribution-NonCommercial-ShareAlike 4.0 International
Download date	2026-05-09 16:53:29
Item License	http://creativecommons.org/licenses/by-nc-sa/4.0/
Link to Item	https://hdl.handle.net/20.500.14519/1923

Correlator-based multipath detection technique for a global positioning system/GNSS receiver

ISSN 1751-8784

Received on 19th August 2017

Revised 1st March 2018

Accepted on 24th March 2018

E-First on 17th April 2018

doi: 10.1049/iet-rsn.2017.0379

www.ietdl.org

Elie Amani^{1,2,3} ✉, Karim Djouani^{1,3}, Jean-Rémi De Boer², Anish Kurien³, Willy Vigneau²

¹LISSI Lab, University Paris-Est Créteil, 122 rue Paul Armangot, Vitry sur Seine, France

²M3 Systems, 26 rue du Soleil Levant, Lavernose Lacasse, France

³F'SATI/Department of Electrical Engineering, Tshwane University of Technology, 01 Staatsartillerie Road, Pretoria, South Africa

✉ E-mail: amani.kikongo@gmail.com

Abstract: Multipath (MP) is one of the main sources of errors in obtaining precise positioning using global navigation satellite systems (GNSSs) and continues to be extensively studied. In this study, a fast Fourier transform-based MP detection technique is proposed. The detector is formulated as a binary hypothesis test under the assumption that the MP exists for a sufficient time frame that allows its detection. The detection is based on the quadrature arm of the early-minus-late correlator output (Q_{EmL}) for a scalar tracking loop or on the quadrature (Q_{EmL}) and/or in-phase arm (I_{EmL}) for a vector tracking loop, using an observation window of N samples. Performance analysis of the proposed detector is done on multiple-ray (up to around 50) MP signals acquired from the MP environment simulator developed by the German Aerospace Centre (DLR in German). Both scalar and vector tracking schemes are used. The application of the detection test to exclusion of MP contaminated satellites from the navigation solution calculation significantly improves positioning accuracy as well as vector tracking performance. This detection technique can be extended to other GNSSs such as GLONASS, Galileo, and Compass with minor adjustments.

1 Introduction

Multipath (MP) remains one of the main sources of errors in obtaining precise positioning using the global positioning system (GPS) and all other global navigation satellite systems (GNSS). GPS pseudo-range and delta-range measurements can be harshly compromised by MP signals. In fact, MP signals destroy the correlation function shape used for time delay estimation. Several signal processing techniques have been developed to deal with errors induced by MP signals in a GPS receiver. Three classes of techniques can be distinguished. The first class relies on detection of MP. No mitigation is performed but the satellite whose line-of-sight (LOS) signal is absent or severely affected by secondary paths is excluded from the calculation of the navigation solution. Some methods that fall under this class are the early late phase-based MP detection [1, 2], the analysis of variance-based MP detection [3, 4], MP detection using elevation enhanced maps [5], MP detection based on the sequence of successive-time double-differences [6], MP detection based on the analysis of signal-to-noise ratio (SNR) fluctuation [7], MP detection using asymmetry in the slopes of the received signal correlation peak [8], MP detection based on code minus carrier delta-range measurement [9], and MP detection using quickest detection theory [10]. The second class of techniques alters the receiver tracking loop to make it resistant to MP signals. Some techniques that fall under this class include the narrow correlator [11], the edge correlator [12], the strobe correlator [12], the high-resolution correlator [13], the gated correlator [14], the MP elimination technology [15], the a-posteriori MP estimation technique [16] and the non-linear Bayesian tracking loops [17]. The third class is based on joint detection and estimation of the LOS and/or MP signal parameters (amplitude, delay, and phase). Examples include the MP estimating delay lock loop [18], the modified rake delay lock loop [19], the MP mitigation technology [20], the vision correlator [21], the fast iterative maximum-likelihood algorithm [22, 23], deconvolution approaches [24, 25], and frequency domain processing [26, 27].

The approach that is suggested in this paper is a MP detection technique. It has been partly introduced in [28]. The contribution comes from the special use of the early-minus-late (EmL) correlator output and the specification of a frequency domain

detection metric. As the detector exploits the EmL correlator output, it is thus based on the detection of a bias on the estimated code delay but using the post-correlation raw measurement. For the case of low-receiver dynamics, the impact of these biases may be attenuated in a receiver that utilises a narrow discriminator and more if the receiver operates in vector tracking mode and in tight coupling with an inertial navigation system. For the case of medium or high-receiver dynamics, the code delay errors are spread in the frequency domain as the receiver velocity is high. Power measurements that are obtained from a fast Fourier transform (FFT)-based power spectral density (PSD) estimator are therefore interesting. The PSD estimator being able to spot power increase on the EmL output due to MP presence, a detector based on it may therefore rightly be utilised to exclude MP contaminated measurements from the navigator or to control the covariance matrix of delay and Doppler measurements in the navigator. The detector is defined under the assumption that the delay locked loop (DLL) is implemented conjointly with a phase locked loop (PLL) that is in the lock. Furthermore, the detector is defined by considering that the EmL correlator output discriminatory nature will eliminate some of the non-MP interferences that might also affect it apart from MP. In fact, the EmL output is a discriminator on its own and it reduces somehow the effects of interference, but that depends on the early-late chip spacing and on the autocorrelation function shape. Also, MP is a type of interference on its own. Depending on whether it is specular or diffuse, it impacts the carrier to noise ratio (C/N_0) as narrowband or wideband interference. The proposed FFT-based detector basically aims at detecting any channel that is contaminated by MP or interference. This paper thus also seeks to show that multipath interference is the one that mostly mirrors its effect on the EmL output through experimental results using data from the DLR multipath model.

The detector is used to exclude MP affected satellites from the calculation of the position, velocity, and time (PVT) solution. This approach is, therefore, a post-correlation level anticipatory measure in comparison with fault detection and exclusion methods and integrity monitoring methods that are used in the navigator as in [29–31]. Also, MP estimation techniques, especially those based on

frequency domain processing, may present a high-computational burden in comparison with MP detection techniques. Moreover, MP mitigation that is based on the estimation of the delay and Doppler frequency of MP signals undergoes the measurement errors at the output of discriminators [32–34]. MP parameters estimation accuracy depends on the kind of discriminator that is used, the noise bandwidth of tracking loops, and the tracking loop configuration, which do not always take MP presence into account. Adding to this is the fact that many satellite constellations can now be jointly used to obtain the PVT solution in one GNSS receiver. Thus, excluding MP contaminated satellites instead of spending computational resources to mitigate MP, especially in a vector tracking context, can be a more suitable approach.

A detection test is proposed for both scalar tracking loop (STL) and vector tracking loop (VTL). The test metrics are defined using correlator outputs. For the STL, the quadrature arm of the EmL correlator output is used in the detector metric. Indeed, for an STL, depending on the relative phase of the MP signal, the presence of MP increases the signal power on the quadrature arm of the EmL correlator output (Q_{EmL}) in comparison with the power that is usually observed in the absence of MP. This increase in signal power is used to detect MP with the specification of a proper threshold. For a VTL both the in-phase and quadrature arms of the EmL correlator output are utilised in the detector metric. In fact, for a VTL with a navigator that is not contaminated, the increase in signal power due to the presence of MP may occur on the in-phase arm (I_{EmL}) and/or on the quadrature arm (Q_{EmL}) of the EmL correlator output depending on the delay and phase of the MP signal. In this study, the tracking scheme that is used for the experiments conducted using DLR MP data is a vector delay frequency locked loop and a PLL aided by the navigator, with the possibility to switch to a scalar DLL and a frequency-assisted PLL.

The rest of the paper is organised as follows. Section 2 presents the MP model that was used to theoretically assess the performance of the proposed detection technique before applying it to DLR MP data. Section 3 explains the link between correlator outputs and MP detection. In Section 4, the detection approach used for the proposed detector is described in detail. Section 5 describes the experimental setup, meaning the GPS software receiver that is used to run simulations. Section 6 describes the DLR MP model and the way the data used for experiments were generated. Experimental results are provided in Section 7. Section 8 gives concluding remarks.

2 MP model and correlator outputs

In the presence of MP, the low-pass signal entering the correlators of a GPS tracking channel, neglecting the low-rate data, depends on the amplitude, code delay, carrier phase, and frequency of LOS and MP signals and can be expressed as

(see (1)),

where $\varphi_l(t) = \varphi_l(0) + 2\pi \int_0^t f_l(u) du$, L is the number of MP signals, $A_0 = \sqrt{2P_0}$ and $A_l = \sqrt{2P_l}$ are the LOS and l th MP amplitudes, P_0 , P_l , and f_l are, respectively, the power of the LOS, the power, and frequency of the l th MP signal, $C(t)$ is the code division multiple access spreading code, τ_0 , τ_l , φ_0 , and φ_l are the time and phase delays induced by the transmission from satellite to receiver for the LOS and l th MP signals, respectively, ω is the nominal GPS L1 radial frequency, and $w(t)$ is the zero-mean additive white Gaussian noise (AWGN) with variance σ^2 . Each tracking channel constitutes a filter that matches the satellite that is allocated. This matched filter correlates the received signal, sampled at $F_s = 1/T_s$, with a local replica. The signal at the output of the prompt correlator at an instant of time $t_n = \sum_{m=0}^n T_m$, obtained after a coherent integrate-and-dump operation of duration T_n , can be expressed as

(see (2)),

where $R(\cdot)$ is the correlation function, $\Delta\tau_{0,n}$ is the error between the LOS signal delay and the estimated code replica delay, $\Delta f_{0,n}$ and $\Delta f_{l,n}$ are the errors between the LOS (respectively, the l th MP) carrier frequency and the estimated carrier replica frequency, $\Delta\varphi_{0,n}$ is the error between the LOS carrier phase and the estimated carrier replica phase, $\delta_{l,n}$ is the delay of the l th MP with respect to the LOS, $\theta_{l,n}$ is the phase shift of the l th MP with respect to the LOS, and $w_p[n]$ is the post-correlation AWGN. The EmL correlator output, at an instant of time t_n , can be expressed as

(see (3)),

where d is half the early-late chip spacing $\partial = 2d$ ($0 < \partial \leq 1$) in chips. For simplicity in the correlator outputs notation and ease of theoretical analysis, it is considered that all MP signals can combine into a single effective MP. The EmL in-phase and quadrature outputs can, therefore, be rewritten as

(see (4a)),

(see (4b)), where the subscript M refers to the MP resulting from a vector combination of all MP signals that are present, $A_0 = \sqrt{2P_0}(\sin(\pi\Delta f_{0,n}T_n)/\sin(\pi\Delta f_{0,n}T_s))$, and $A_M = \sqrt{2P_M}(\sin(\pi\Delta f_{M,n}T_n)/\sin(\pi\Delta f_{M,n}T_s))$.

For a VTL in lock with enough healthy channels (non-contaminated by MP), it can be assumed that the error on the DLL

$$x(t) = A_0 C(t - \tau_0) \exp[j\varphi_0(t)] + \sum_{l=1}^L A_l C(t - \tau_l) \exp[j\varphi_l(t)] + w(t), \quad (1)$$

$$I_p[n] + jQ_p[n] = \sqrt{2P_0} R(\Delta\tau_{0,n}) \frac{\sin(\pi\Delta f_{0,n}T_n)}{\sin(\pi\Delta f_{0,n}T_s)} \exp(j\Delta\varphi_{0,n}) + \sum_{l=1}^L \sqrt{2P_l} R(\Delta\tau_{0,n} - \delta_{l,n}) \frac{\sin(\pi\Delta f_{l,n}T_n)}{\sin(\pi\Delta f_{l,n}T_s)} \exp[j(\Delta\varphi_{0,n} - \theta_{l,n})] + w_p[n], \quad (2)$$

$$I_{EmL}[n] + jQ_{EmL}[n] = \sqrt{2P_0} [R(\Delta\tau_{0,n} + d) - R(\Delta\tau_{0,n} - d)] \times \frac{\sin(\pi\Delta f_{0,n}T_n)}{\sin(\pi\Delta f_{0,n}T_s)} \exp(j\Delta\varphi_{0,n}) + \sum_{l=1}^L \sqrt{2P_l} \times [R(\Delta\tau_{0,n} - \delta_{l,n} + d) - R(\Delta\tau_{0,n} - \delta_{l,n} - d)] \frac{\sin(\pi\Delta f_{l,n}T_n)}{\sin(\pi\Delta f_{l,n}T_s)} \exp[j(\Delta\varphi_{0,n} - \theta_{l,n})] + w_{EmL}[n], \quad (3)$$

$$I_{EmL}[n] = A_0 [R(\Delta\tau_{0,n} + d) - R(\Delta\tau_{0,n} - d)] \cos(\Delta\varphi_{0,n}) + A_M [R(\Delta\tau_{0,n} - \delta_{M,n} + d) - R(\Delta\tau_{0,n} - \delta_{M,n} - d)] \cos(\Delta\varphi_{0,n} - \theta_{M,n}) + w_{I,EmL}[n], \quad (4a)$$

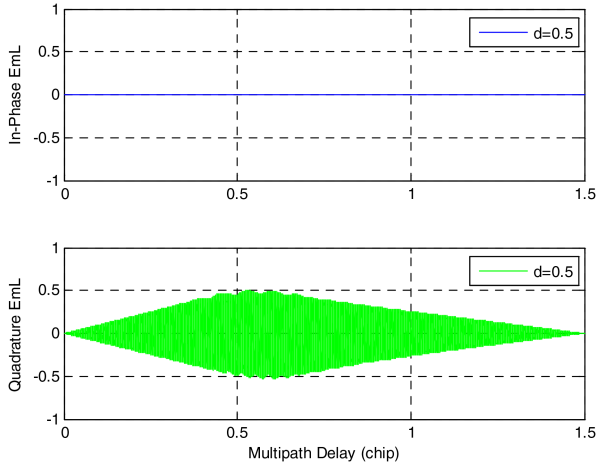


Fig. 1 I_{EmL} and Q_{EmL} amplitudes versus MP delay (DLL and PLL in the lock); $A_0 = 1$; $\alpha = A_M/A_0 = 0.5$; $d = 0.5\text{chip}$; $\theta_M = 2\pi f_{L1}\delta_M/R_C$

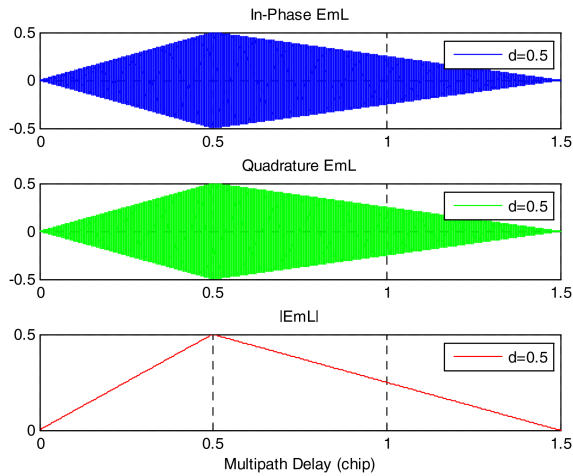


Fig. 2 I_{EmL} , Q_{EmL} and $|EmL|$ amplitudes versus MP delay for VTL in the lock; $A_0 = 1$; $\alpha = A_M/A_0 = 0.5$; $d = 0.5\text{chip}$; $\theta_M = 2\pi f_{L1}\delta_M/R_C$

approaches zero, i.e. that $\Delta\tau_{0,n} \simeq 0$. This means that if it is assumed that there are enough healthy channels such that the navigator can estimate the PVT solution with minimal error, this solution allows correct estimation of the code chip rate in each channel, which implies that $R(\Delta\tau_{0,n} + d) - R(\Delta\tau_{0,n} - d) \simeq 0$ as well. The EmL in-phase and quadrature outputs in the presence of at least one MP contaminated channel, in this case, are given by

$$I_{EmL}[n] = A_M[R(-\delta_{M,n} + d) - R(-\delta_{M,n} - d)]\cos(\Delta\phi_{0,n} - \theta_{M,n}) + w_{I,EmL}[n], \quad (5a)$$

$$Q_{EmL}[n] = A_M[R(-\delta_{M,n} + d) - R(-\delta_{M,n} - d)]\sin(\Delta\phi_{0,n} - \theta_{M,n}) + w_{Q,EmL}[n]. \quad (5b)$$

In the case of an STL (DLL), the quadrature arm of the EmL correlator output (4b) is used in the detector metric that is described in Section 4 because the DLL in lock strives to maintain

the EmL in-phase arm power around zero even in the presence of MP. For a VTL, the complex output of the EmL correlator output is used, i.e. the in-phase and quadrature EmL outputs (5a) and (5b) are considered because the VTL in lock condition would still register signal power on either the in-phase or quadrature arms in the presence of at least one MP contaminated channel before navigator contamination. The complex EmL correlator output, at an instant of time t_n , for a single effective MP, with $\Delta\tau_{0,n} \simeq 0$ and $R(\Delta\tau_{0,n} + d) - R(\Delta\tau_{0,n} - d) \simeq 0$, can be expressed as (see (6)). The justification for the use of in-phase and/or quadrature arms in the detector metric is discussed in the next section.

3 Correlator outputs and MP detection

An analysis of GPS correlator outputs in the absence and in the presence of MP can lead to the design of MP detection techniques. In the absence of MP, the in-phase prompt correlator output carries the LOS signal power.

In the presence of a MP signal, the prompt correlator output is composed of the sum of the LOS and MP signals and the STL locking point is adjusted to this sum. As the tracking loop constantly seeks to bring the quadrature prompt power to an average close to zero, the quadrature prompt output will have part of the LOS + MP signal power only for a short transient time following MP arrival then will get back to an average around zero, especially in low-dynamic scenarios. If the MP signal is in phase or opposition of phase with the LOS signal, the quadrature prompt power will remain close to zero.

The situation in the presence of MP is different for early and late correlator outputs and consequently for in-phase EmL and quadrature EmL outputs as can be observed in Fig. 1 for the STL and in Fig. 2 for the VTL. For the STL (DLL) in lock, in the presence of MP, the signal energy in the in-phase arm of the EmL correlator output is around zero and the energy in the quadrature arm during transient and steady-state times following MP arrival is significantly higher than in the absence of MP, unless the MP signal is in phase or opposition of phase with the LOS signal. In the absence of MP, only noise is observed on the quadrature EmL output.

A zoom on Fig. 1 shows that the Q_{EmL} output in the presence of MP oscillates along the different MP delay values between a maximum and a minimum which depend on the MP to LOS amplitude ratio α and on the early-late chip spacing $\vartheta = 2d$. The Q_{EmL} output is zero when the MP signal is in phase ($\theta_M = 0^\circ + k360^\circ$) or opposition of phase ($\theta_M = 180^\circ + k360^\circ$) with the LOS signal, with k being an integer. These MP phase values ($\theta_M = 0^\circ + k360^\circ$ and $\theta_M = 180^\circ + k360^\circ$) correspond to MP delay values $\delta_M = nR_C/f_{L1}$ and $\delta_M = (n + 0.5)R_C/f_{L1}$, with n being an integer and R_C the code chip rate. Here, the MP phase is related to MP delay using $\theta_M = 2\pi f_{L1}\delta_M/R_C$, i.e. it is assumed that the MP phase is only due to the differential path delay. In general, upon reflection or diffraction, the MP signal undergoes a relative phase θ_M that either can be modelled using the differential path delay and reflector and antenna parameters [35] or else can be assumed to be random [36]. For the VTL with an uncontaminated navigator, both I_{EmL} and Q_{EmL} outputs increase in signal power in the presence of MP as shown in Fig. 2 and when Q_{EmL} is at zero, I_{EmL} is not and vice versa. This means that for all MP phase or delay values, the absolute value $|EmL| = \sqrt{I_{EmL}^2 + Q_{EmL}^2}$ increases in amplitude in the presence of MP.

$$Q_{EmL}[n] = A_0[R(\Delta\tau_{0,n} + d) - R(\Delta\tau_{0,n} - d)]\sin(\Delta\phi_{0,n}) + A_M[R(\Delta\tau_{0,n} - \delta_{M,n} + d) - R(\Delta\tau_{0,n} - \delta_{M,n} - d)]\sin(\Delta\phi_{0,n} - \theta_{M,n}) + w_{Q,EmL}[n], \quad (4b)$$

$$EmL[n] = I_{EmL}[n] + jQ_{EmL}[n] = (I_E - I_L)_n + j(Q_E - Q_L)_n = A_M[R(-\delta_{M,n} + d) - R(-\delta_{M,n} - d)]\exp[j(\Delta\phi_{0,n} - \theta_{M,n})] + w_{EmL}[n]. \quad (6)$$

4 Binary hypothesis tests for MP detection

4.1 Detection test on STL

The detection test is defined based on the fact that in the presence of a specular MP, the signal power on the quadrature arm of the EmL correlator output (Q_{EmL}) increases significantly in comparison with the normal power that is observed in the absence of MP, as discussed in Sections 2 and 3. A binary hypothesis test can, therefore, be defined as follows for an observation window of N samples and of initial index n_0

$$\begin{aligned} H_0: Q_{\text{EmL}}(n) &= w_{Q_{\text{EmL}}}(n), \\ H_1: Q_{\text{EmL}}(n) &= s(n) + w_{Q_{\text{EmL}}}(n), \quad \text{with } n \in \{1, \dots, N\} + n_0. \end{aligned}$$

In other terms, under hypothesis H_0 , no signal is present on the Q_{EmL} output, and only noise is observed which implies that no MP signal is present; whereas under hypothesis H_1 a signal $s(n)$ plus noise are observed, which implies the presence of MP. By assuming that the signal $s(n)$ is a sinusoidal signal, which is the case in general, the design of the MP detector reduces to a problem of detection of a sinusoidal signal in AWGN. The FFT detector [37, 38] that is used in the sonar and radar systems detects the presence of a signal in the frequency domain and can, therefore, be rightly applied to GPS MP detection using the above hypotheses formulation. We propose that the MP detector compute the periodogram as

$$\begin{aligned} \Omega(m) &= \frac{1}{N} |Q_{\text{EmL}}(m)|^2, \quad \text{where} \\ Q_{\text{EmL}}(m) &= \sum_{n=n_0}^{n_0+N-1} Q_{\text{EmL}}(n) e^{-j2\pi mn/N}, \end{aligned} \quad (7)$$

where $Q_{\text{EmL}}(m)$ is the discrete Fourier transform of $Q_{\text{EmL}}(n)$ and is implemented via an N -point FFT algorithm. The MP detector subsequently chooses the largest value of $\Omega(m)$, divides it by the maximum likelihood estimate (MLE) of noise variance $\hat{\sigma}^2$ and then compares the result against a threshold η . The detection test to decide for H_0 or H_1 is therefore formulated as

$$\frac{\max(\Omega(m))}{\hat{\sigma}^2} \underset{H_1}{>} \eta \quad \text{or} \quad \frac{\max(\Omega(m))}{\hat{\sigma}^2} \underset{H_0}{<} \eta, \quad (8)$$

where

$$\begin{aligned} \hat{\sigma}^2 &= \frac{1}{N} \sum_{n=1}^N (Q_{\text{EmL}}(n+n_0) - \bar{Q})^2 \quad \text{and} \quad \bar{Q} \\ &= \frac{1}{N} \sum_{n=1}^N Q_{\text{EmL}}(n+n_0). \end{aligned}$$

The detailed derivation of this detection metric is shown in Appendix 1. This MP detector is optimum if $s(n)$ is a sinusoid. This sinusoid may have unknown amplitude, phase and/or frequency, but optimality requires the frequency to be a bin frequency, i.e. to be equal to $2\pi m/N$, with m being an integer. Optimum detection entails that for a given probability of false alarm (PFA), the detector gives the maximum probability of detection (PD).

The detection threshold is (see Appendix 2 for derivation):

$$\eta = \exp\left\{\frac{[\text{cdf}^{-1}(1 - \text{PFA}/2)]^2}{N}\right\} - 1, \quad (9)$$

where cdf is the cumulative distribution function of the standard normal distribution, cdf^{-1} is the inverse cumulative distribution function, and the PFA. The values of PFA and N have a great impact on the performance of the detector, and there is a trade-off between obtaining a high-detection capability and a low false alarm rate. Increasing the value of N and/or PFA improves the detection capability of the detector in theory. However, in practice, increasing the value of N delays the instant, after system initialisation, when the MP is detected and increases the complexity of the N -point FFT computation. On the other hand, increasing PFA may result in many false detection and this may not be beneficial if the objective is to exclude the MP contaminated satellites from the navigation solution. One might wind up with fewer satellites than needed to compute the PVT solution within acceptable precision ranges. If N is assumed sufficiently large ($N > 32$), the PD is given by [37]

$$\begin{aligned} \text{PD} &= 2 - \text{cdf}\left(\text{cdf}^{-1}\left(1 - \frac{\text{PFA}}{2}\right) - \sqrt{\text{SNR}}\right) \\ &\quad - \text{cdf}\left(\text{cdf}^{-1}\left(1 - \frac{\text{PFA}}{2}\right) + \sqrt{\text{SNR}}\right), \end{aligned} \quad (10)$$

where SNR is the post-correlation SNR of the Q_{EmL} output and is given by $\text{SNR} = NA^2/2\sigma^2$. This PD depends on the chosen PFA, on the amplitude A of the signal $s(n)$ on the Q_{EmL} output, and on the noise power on that output. This noise power is given by $\sigma^2 = \sigma_n^2 K(1-r)$ [11] where $\sigma_n^2 = N_0 f_s$ is the thermal noise power (N_0 and f_s are noise spectral density and baseband sampling frequency, respectively), K is the number of correlation points, and $r = 1 - 2d$ is the level of correlation between the early and late outputs, d being half the early-late chip spacing. Taking $A_M = \alpha A_0$ in (4b) and ignoring the index n (indicating samples), the amplitude A of the signal $s(n)$ is given by

$$\begin{aligned} A &= A_0 \\ &\left\{ \begin{aligned} &[R(\Delta\tau_0 + d) - R(\Delta\tau_0 - d)]\sin(\Delta\varphi_0) \\ &+ \alpha[R(\Delta\tau_0 - \delta_M + d) - R(\Delta\tau_0 - \delta_M - d)]\sin(\Delta\varphi_0 - \theta_M) \end{aligned} \right\}, \end{aligned}$$

where $A_0 = \sqrt{CK} \sin c(\pi\Delta f T)$ with C being the LOS power before correlation, T the coherent integration time ($K = T f_s$) and Δf the error between the LOS carrier frequency and the estimated carrier replica frequency. The post-correlation SNR at the Q_{EmL} output has thus the following expression linking it to the C/N_0 : (see (11)). Fig. 3 illustrates the PD given different PFA values for different values of SNR. It can be observed that a high-SNR (consequently high C/N_0) value increases PD and theoretically the performance of the MP detector.

4.2 Detection test on VTL

For the VTL, the presence of a specular MP is visible on both the in-phase and quadrature arms of the EmL correlator output (Q_{EmL}) if the navigator is not contaminated. The suggested test is like the one defined for the STL but considers the complex output of the EmL correlator output.

A binary hypothesis test can be defined as follows for an observation window of N samples and of initial index n_0

$$\begin{aligned} H_0: \text{EmL}(n) &= w_{\text{EmL}}, \\ H_1: \text{EmL}(n) &= s(n) + w_{\text{EmL}}, \quad \text{with } n \in \{1, \dots, N\} + n_0. \end{aligned}$$

$$\begin{aligned} \text{SNR} &= \frac{NA^2}{2\sigma^2} = \frac{C}{N_0} \frac{NT \sin^2(\pi\Delta f T)}{2d} \\ &\times \left\{ \begin{aligned} &[R(\Delta\tau + d) - R(\Delta\tau - d)]\sin(\Delta\varphi) \\ &+ \alpha[R(\Delta\tau - \delta_M + d) - R(\Delta\tau - \delta_M - d)]\sin(\Delta\varphi - \theta_M) \end{aligned} \right\}^2. \end{aligned} \quad (11)$$

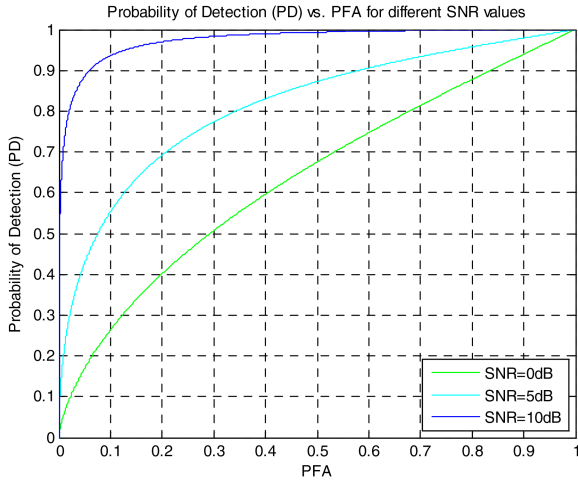


Fig. 3 Probability of MP detection versus PFA for different SNRs

As in the STL case, the detector computes the periodogram but this time based on the complex FFT

$$\Omega(m) = \frac{1}{N} |\text{EmL}(m)|^2, \quad \text{where} \quad (12)$$

$$\text{EmL}(m) = \sum_{n=n_0}^{n_0+N-1} \text{EmL}(n) e^{-j2\pi mn/N}.$$

$\text{EmL}(m)$ is the discrete complex Fourier transform of $\text{EmL}(n) = I_{\text{EmL}}(n) + jQ_{\text{EmL}}(n)$. The detector then chooses the largest value of $\Omega(m)$, divides it by the MLE of noise variance $\hat{\sigma}^2$ and then compares the result against a threshold η . The detection test to decide for H_0 or H_1 is therefore formulated as

$$\frac{\max(\Omega(m))}{\hat{\sigma}^2} > \eta \quad \text{or} \quad \frac{\max(\Omega(m))}{\hat{\sigma}^2} < \eta, \quad (13)$$

where $\hat{\sigma}^2 = (1/N) \sum_{n=1}^N |\text{EmL}(n+n_0) - \overline{\text{EmL}}|^2$ and $\overline{\text{EmL}} = (1/N) \sum_{n=1}^N \text{EmL}(n+n_0)$.

The detection threshold is still

$$\eta = \exp\left\{\frac{[\text{cdf}^{-1}(1 - \text{PFA}/2)]^2}{N}\right\} - 1.$$

5 Experimental setup: simulation methodology

For evaluating the performance of the detector described in the previous section, MATLAB simulations are performed using a software GPS receiver simulator whose architecture is depicted in Fig. 4. This is a federated (decentralised) architecture, meaning that each tracking channel has a local estimation filter of the Kalman family, referred to here as a local estimator. All channels deliver their measurements to the navigator, which is the master PVT estimation filter. This receiver is made of a bank of correlators, discriminators, local estimators (based on a fixed gain Kalman filter algorithm), code and carrier numerically controlled oscillators (NCOs), and a navigator based on an extended Kalman filter (EKF) algorithm. The navigator provides feedback information to code and carrier NCOs. The DLR MP model is utilised in the trajectory and environment simulator used as the signal source. This vector tracking system is enhanced by adding the proposed correlator-based MP detector and a C/N_0 estimator that allow the navigator to exclude unhealthy satellites from PVT computation. This receiver has the potential to perform scalar tracking and vector tracking.

The used C/N_0 estimator [39] is based on the second- and fourth-order moments of the input process to obtain a separate estimation of the carrier and noise strengths. Let $s[n] = I_p[n] + jQ_p[n]$ be the complex signal (process) at the prompt correlator output. The theoretical formulation of the second- and

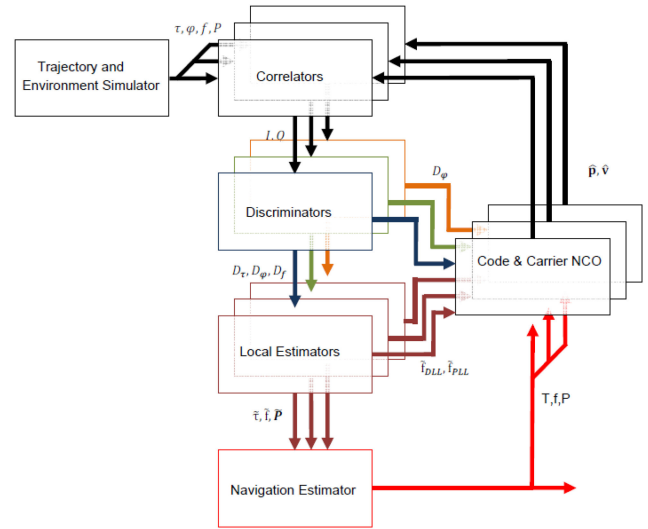


Fig. 4 Software GPS receiver simulator architecture

fourth-order moments of this process is $M_2 = E\{|s[n]|^2\}$ and $M_4 = E\{|s[n]|^4\}$. Based on these moments, signal power and noise power are defined as $P_s(M_2, M_4) = \sqrt{2M_2^2 - M_4}$ and $P_n(M_2, M_4) = M_2 - P_s(M_2, M_4)$, respectively. The statistical moments M_2 and M_4 are estimated by their respective averages

$$\hat{M}_2 = \frac{1}{N} \sum_{l=1}^N |s[l]|^2 \quad \text{and} \quad \hat{M}_4 = \frac{1}{N} \sum_{l=1}^N |s[l]|^4. \quad (14)$$

Also, the C/N_0 estimate is, therefore

$$\frac{C}{N_0} = \frac{\hat{P}_s(\hat{M}_2, \hat{M}_4)}{\hat{P}_n(\hat{M}_2, \hat{M}_4)}. \quad (15)$$

A threshold of 30 dB-Hz is chosen, meaning that the satellites whose received signal has an estimated C/N_0 that is <30 dB-Hz will be excluded from PVT calculation.

6 DLR MP data used for experiments

This section briefly explains how the synthesised MP data that are used for experiments in this work were generated via simulations using the DLR MP Model software.

6.1 DLR MP model

The DLR model is a software tool developed under MATLAB by the German Aerospace Center (DLR) to allow characterisation of the propagation channel for wideband signals such as GNSS signals. The innovative aspect of this model is the synthesis of statistical data from measurements obtained with deterministic scenarios. Measurements campaigns were performed in Munich in 2002 using wideband signals (100 MHz) modulated on carriers in the GNSS band, specifically between 1460 and 1560 MHz (close to GPS L1). The resulting transmitter was embedded in a Zeppelin that simulated a moving satellite at an altitude of 4 km. A vehicle circulated around Munich's streets from the urban canyon to narrow suburban streets with momentary open sky boulevards, following the Zeppelin displacement. The latter disappeared and appeared behind buildings and obstacles that surrounded the vehicle's trajectory which was assumed to be a straight line locally. The deterministic aspect of the DLR model intervenes in the direct path (LOS) modelling and the calculation of the echoes (MP) parameters evolution. The statistical aspect comes from the number of generated echoes, their lifetime, and the position and the attenuation factor of reflectors. The echoes lifetime follows a probability distribution whose parameters are deduced from measurements. The attenuation due to a reflector, its bandwidth, its

Table 1 Constellations simulated with the DLR model

	constellation example no. 1			constellation example no. 2		
date and time	01/03/2013 from 16:50 to 16:58			04/03/2013 from 08:50 to 08:56		
position	2.23894°E/48.88341°N			2.23894°E/48.88341°N		
visible GPS satellites represented by their pseudorandom noise (PRN) code IDs	PRN	elevation	azimuth	PRN	elevation	azimuth
	05	+48.6	198.0	01	+78.5	98.5
	07	+12.1	61.4	17	+32.0	308.9
	15	+41.8	294.5	23	+21.9	183.8
	21	+11.5	307.7	14	+16.2	38.4
	28	+53.7	106.0	28	+12.2	259.1
	08	+41.8	56.5	20	+69.3	252
	09	+55.7	249.4	11	+53.6	137.9
	27	+30.0	248.0	32	+78.9	62.1
	26	+82.9	353.7			

Table 2 Summary of satellites visibility/masking statistics

Environment	Dynamics	Trajectory	Constellation	No LOS masking (MPs)	LOS + Partial LOS masking (LOS + MPs)	Total LOS masking (MPs)	
suburban	pedestrian	fixed point	no. 1	3 (33%)	4 (44%)	2 (22%)	
			no. 2	1 (12%)	7 (88%)	0	
		straight line	no. 1	4 (44%)	5 (56%)	0	
			no. 2	4 (50%)	4 (50%)	0	
			90° turn	no. 1	4 (44%)	5 (56%)	0
				no. 2	4 (50%)	4 (50%)	0
	vehicle (Car)	fixed point	no. 1	3 (33%)	5 (56%)	1 (11%)	
			no. 2	4 (50%)	3 (37%)	1 (12%)	
		straight line	no. 1	3 (33%)	6 (67%)	0	
			no. 2	3 (37%)	5 (63%)	0	
			90° turn	no. 1	5 (56%)	4 (44%)	0
				no. 2	3 (37%)	5 (63%)	0
urban	pedestrian	fixed point	no. 1	4 (44%)	3 (33%)	2 (22%)	
			no. 2	6 (75%)	1 (12%)	1 (12%)	
		straight line	no. 1	3 (33%)	3 (33%)	3 (33%)	
			no. 2	2 (25%)	6 (75%)	0	
			90° turn	no. 1	2 (22%)	7 (78%)	0
				no. 2	3 (37%)	5 (63%)	0
	vehicle (Car)	fixed point	no. 1	3 (33%)	3 (33%)	3 (33%)	
			no. 2	4 (50%)	4 (50%)	0	
		straight line	no. 1	3 (33%)	4 (44%)	2 (22%)	
			no. 2	5 (63%)	2 (25%)	1 (12%)	
			90° turn	no. 1	4 (44%)	5 (56%)	0
				no. 2	4 (50%)	4 (50%)	0

fading factor (Rician factor) and its lifetime (the lifetime of the echo it generates) are statistically determined from the measurement campaigns. The echoes delays and phases evolve following the relative movement of the vehicle with respect to the position of the reflectors.

6.2 Presentation of data simulated by the DLR software

An analysis of harsh environments as they can be defined by the DLR model (suburban and urban) for several types of trajectories (fixed point, straight line displacement, displacement with a 90° turn) and for two types of dynamics (pedestrian and vehicle) has been realised by the authors. Simulations of 60 s duration have been performed for two real constellations to confirm the statistical validity of results. The constellation details are depicted in Table 1.

The simulations performed with the DLR model made it possible to reconstruct realistic conditions experienced in harsh environments. Table 2 summarises the statistics of satellites visibility/masking for different environments, dynamics, trajectories, and constellations. For each of the two constellations, the number of satellites that undergo either no LOS masking or

partial LOS masking or total LOS masking is shown. For all these cases, MP is present.

6.3 DLR data scenarios used in experiments

Table 3 summarises some data scenarios from the DLR model simulations that are used in the experiments performed to validate the proposed MP detector and vector tracking solution.

7 Experimental results

The numerous MP environment scenarios that the DLR model software can generate are used to evaluate the performance of the proposed detection technique. The scenarios depicted in the figures and/or tables hereafter involve a pedestrian or a vehicle moving parallel to the buildings in urban or suburban environments. Figs. 5 and 6 are examples of the behaviour of the detector in the presence and in the absence of MP signals for both the scalar and vector tracking loops. Subfigures (a), (b) and (c) depict the parameters (amplitude, phase, and delay) of the different signal paths (LOS and MP) for two of the scenarios under study. Amplitude values are normalised, with the LOS amplitude having a maximum value of 1 (0 dB). The LOS amplitude is represented in blue. The LOS

Table 3 Scenarios of DLR data used for experiments

constellation	constellation no. 1					
environment	suburban			urban		
Trajectory	straight line			straight line		
dynamics	pedestrian		vehicle	pedestrian		vehicle
	constant acceleration	constant velocity	constant velocity	constant acceleration	constant velocity	constant velocity
	(0.5 m/s ²)	(50 km/h)	(90 km/h)	(0.5 m/s ²)	(50 km/h)	(90 km/h)
Scenarios	scenario 1	scenario 2	scenario 3	scenario 4	scenario 5	scenario 6

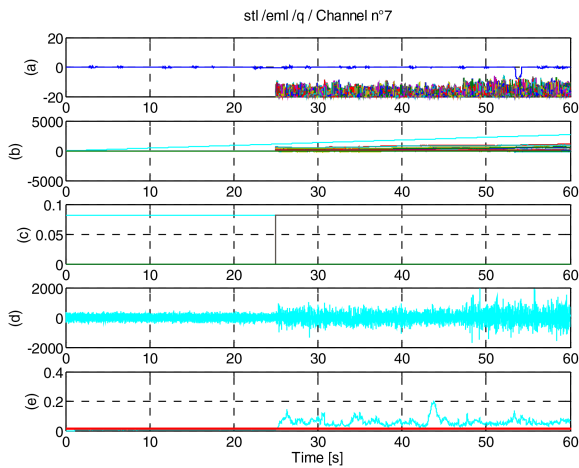


Fig. 5 Scenario 5 – moving vehicle (50 km/h) – urban environment, channel 7 (PRN09)
 (a) LOS and MP amplitudes in dB, (b) LOS and MP phases in rad, (c) LOS and MP delays in s, (d) Quadrature EmL power, (e) Detector metric and threshold (STL, $N = 1024$, PFA = 10^{-4} , estimated $C/N_0 = 45$ dB-Hz, then around 40 dB-Hz in the presence of MP)

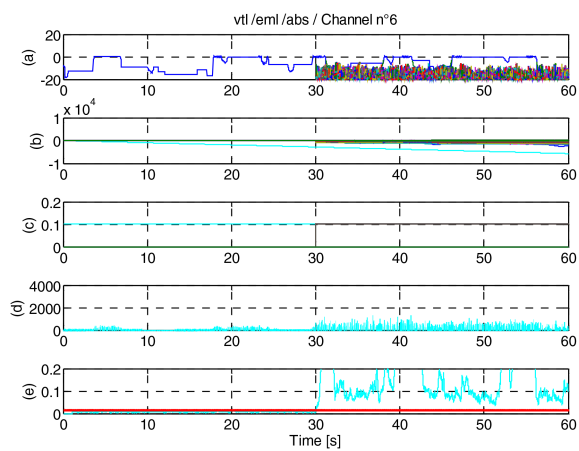


Fig. 6 Scenario 2 – moving vehicle (50 km/h) – suburban environment, channel 6 (PRN08)
 (a) LOS and MP amplitudes in dB, (b) LOS and MP phases in rad, (c) LOS and MP delays in s, (d) |EmL| power, (e) Detector metric and threshold (VTL, $N = 1024$, PFA = 10^{-4} , estimated $C/N_0 = 45$ dB-Hz, then around 40 dB-Hz in the presence of MP)

phase and delay parameters are represented in cyan colour. The two scenarios from the DLR MP environment simulator are defined to allow MP to appear around the 25th tracking second in Fig. 5 for the STL – Channel 7 (PRN09) and around the 30th second in Fig. 6 for the VTL – Channel 6 (PRN08). Subfigures (d) and (e) show that the detector performs as expected. The test metric values start below the threshold for the 25 (respectively, 30) tracking seconds where only the LOS signal is present then go above threshold around the 25th (respectively, 30th) second and the rest of the time. This is in accordance with the signal power increase on the Q_{EmL} arm (STL case) and the increase in the absolute value of EmL (VTL case) which also occur around the 25th (respectively, 30th) tracking second.

Table 4 Chosen practical PFA (threshold) values

	STL	VTL
PFA (threshold)	10^{-4} or 10^{-3}	10^{-4} or 10^{-3}

Table 5 Summary of the detector statistical performance

Tracking loop	STL, %	VTL, %
% FA		
pedestrian urban (0.5 m/s ²)	1.18	6.95
vehicle urban (90 km/h)	0.79	0.20
pedestrian suburban (0.5 m/s ²)	1.14	9.23
vehicle suburban (50 km/h)	0.47	3.11
vehicle suburban (90 km/h)	1.05	1.12
% MD		
pedestrian urban (0.5 m/s ²)	4.11	3.72
vehicle urban (90 km/h)	0.39	0.29
pedestrian suburban (0.5 m/s ²)	0.37	0.97
vehicle suburban (50 km/h)	0.94	0.15
vehicle suburban (90 km/h)	0.40	0.46

More experiments are conducted for different DLR MP scenarios (environment-trajectory-dynamics) to statistically formulate the expected percentages of false alarms (% FA) and percentages of missed detection (% MD) for the proposed detector applied to both STL and VTL tracking schemes. Based on these experimental results, the PFAs (thresholds) in Table 4 have been chosen as practical for maximising the detection ability of the detector. The recorded % FA and % MD with these chosen threshold values used on different DLR MP scenarios are summarised in Table 5.

Table 5 shows for the examined scenarios that the maximum % FA is 9.23% and the maximum % MD is 4.11%. The average % FA is 2.41% and the average % MD is 1.18%. These numerical figures show that the proposed detector exhibits good performance and can rightly be used to spot MP effect in a GNSS receiver.

The solution proposed in this study is mostly appropriate for a multi-constellation receiver. In a multi-constellation setting, the number of potentially available satellites is high. Consequently, at a PVT calculation instant of time t_n , there is a high probability to have a reasonable number of satellites that are unaffected by MP and that can be used in the PVT. If the number of healthy satellites decreases significantly, the MP detector threshold can be momentarily raised or the EKF algorithm can be set to base its PVT on prediction until better measurement conditions are restored. The proposed detector is tested in a GPS receiver first (see Constellation No. 1). To create scenarios that will allow comparison between a vector tracking architecture that uses signal quality indicators (a C/N_0 estimator and an MP detector) to exclude MP affected satellites and one that does not, Scenarios 1 to 6 (see Table 3) are slightly modified in experimental simulations. The modification allows only 4 out of 9 available satellites to undergo MPs. Although the five remaining satellites are not MP affected, they do undergo LOS masking occasionally according to the DLR environment settings.

Fig. 7a depicts earth centred earth fixed (ECEF) position and velocity errors for Scenario 1 for the VTL tracking scheme, without the use of the C/N_0 estimator and MP detector, i.e. without unhealthy channel exclusion from PVT calculation (red lines) and then with the use of a C/N_0 estimator and MP detector, i.e. with

unhealthy channel exclusion (black lines). Table 6 provides numerical values of error means and standard deviations (STD) for Scenarios 1 and 3. It can be observed that the magnitude of positioning errors (position and velocity) when there is no exclusion (peaks in the hundreds of metres or metres/second) is far bigger than when there is an exclusion (average of a few metres or metres/s).

Fig. 7b, which shows position and velocity errors for Scenario 2 demonstrates that under very harsh MP conditions, the EKF algorithm in the navigator may diverge. However, the exclusion of MP contaminated satellites from PVT calculation corrects this divergence problem and improves the PVT accuracy from a magnitude of kilometres and km/s to a few metres and m/s. Fig. 7c shows, for Scenario 6, the number of satellites that are considered healthy by the quality indicators at each PVT computation time and that are therefore included in the calculation. Out of the 9 visible satellites of Constellation 1, the number of used satellites is varying between 4 and 9.

The improvement of PVT accuracy from the exclusion of unhealthy satellites has an interesting consequence: it improves

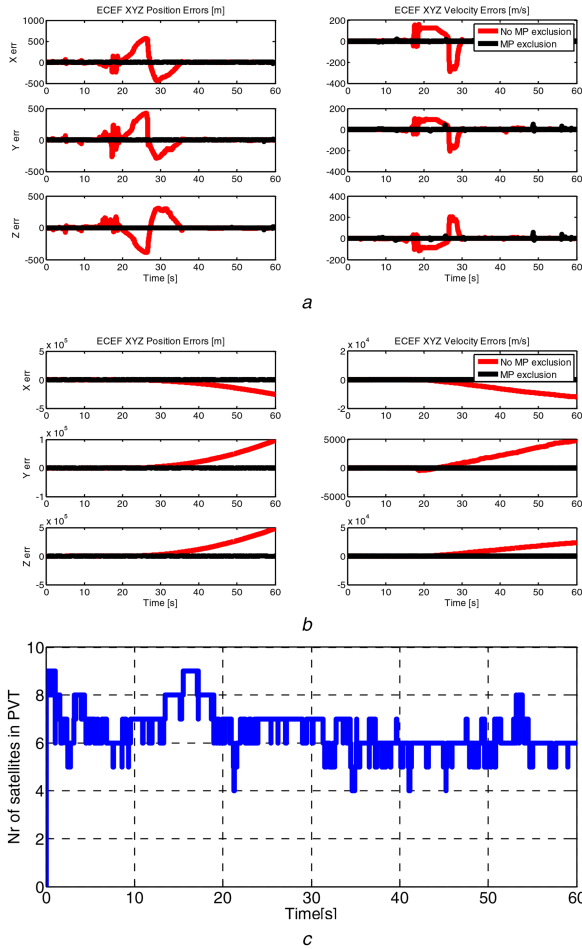


Fig. 7 Positioning performance (a) Scenario 1, VTL ECEF position and velocity errors, (b) Scenario 2, VTL ECEF position and velocity errors, (c) Scenario 6, VTL, number of satellites used in PVT

Table 6 Scenarios 1 and 3, VTL (MP exclusion) versus VTL (no MP exclusion): PVT errors

Error		Scenario 1				Scenario 3			
		Exclusion		No exclusion		Exclusion		No exclusion	
		Mean	STD	Mean	STD	Mean	STD	Mean	STD
Position, m	X	-0.0958	1.4800	-2.7000	167.8853	-0.0035	0.0540	-18.9066	59.6467
	Y	0.0962	1.0371	6.3050	118.3508	0.0072	0.0674	-14.6505	81.2515
	Z	0.0338	1.4036	6.9688	120.2087	-0.0041	0.0797	0.3135	81.5465
Velocity, m/s	X	-0.0850	1.2734	5.6048	62.9437	0.0016	0.2334	0.5553	3.5128
	Y	0.1861	2.6874	4.5766	43.2995	0.0054	0.2396	0.7804	5.0903
	Z	0.1978	2.8808	-3.4923	44.2826	0.0011	0.3011	0.0946	3.8671

vector tracking performance because the estimation of tracking parameters benefits from a more accurate PVT. It should be mentioned that although MP contaminated satellites are excluded from PVT calculation, they continue being tracked by the VTL. Subfigures (a), (b) and (c) of Fig. 8 illustrate code delay, carrier phase and carrier frequency tracking errors of six satellites of Constellation 1 before exclusion of unhealthy satellites from PVT (red lines) and after exclusion (black lines). It is clearly observed that in general, the magnitude of tracking errors decreases as PVT accuracy improves. This is particularly noticeable for the phase tracking errors.

The improvement in carrier phase tracking is a very useful result as it improves the VTL capability to perform carrier suppression and achieve navigation data demodulation. This feature of the proposed solution is not illustrated as real GPS signals with ephemeris data were not used in the experiments. The use of real GPS signals would confirm this assertion.

The performance of the EKF algorithm and the EKF algorithm used with the proposed MP detector (EKF-DET) is also evaluated based on the root mean square error (RMSE) of their position estimations in Fig. 9. The curves that are provided give a measure of the algorithms convergence time and show their asymptotic behaviour. The figures are based on the mean square error (MSE) value of the three-dimensional position vector defined as follows:

$$\sigma_p^2 = E\{(p - \hat{p})^T(p - \hat{p})\} = \sigma_x^2 + \sigma_y^2 + \sigma_z^2,$$

where σ_x^2 , σ_y^2 and σ_z^2 are the MSEs of the ECEF X , Y and Z position coordinates, respectively. The RMSE is therefore computed as $RMSE = \sqrt{\sigma_p^2}$. A corresponding root posterior Cramer–Rao lower bound (PCRLB) that is based on the XYZ position coordinates is similarly computed. This \sqrt{PCRLB} is used as a reference for performance evaluation.

The positioning solutions of the two algorithms are provided for 45 s duration with the navigator operating at a frequency of 100 Hz. Fifty Monte Carlo runs are performed. From Fig. 9, it is clearly observed that the RMSE of the two algorithms is close to each other but the EKF combined with the MP detector (EKF-DET)'s error is lower. In fact, the EKF-DET algorithm's RMSE curve is closer to the PCRLB than the EKF RMSE curve, meaning that it exhibits better performance.

8 Conclusion

This study has suggested an FFT-based MP detection technique for a GPS/GNSS receiver. The application of the detection technique to GNSS synthesised signals on correlator outputs of the code and carrier tracking loops (scalar or vector tracking loops) demonstrate its efficiency in detecting MP contaminated tracking channels. The proposed detector together with a C/N_0 estimator is applied and utilised as signal quality indicators to exclude MP contaminated satellites from the calculation of the PVT solution with a vector tracking scheme. Consequently, the PVT accuracy improvement is of great significance. ECEF positioning errors improve from hundreds or thousands of metres to a few metres. Furthermore, the improvement in PVT accuracy also reduces code delay, carrier phase, and carrier frequency tracking errors because for a VTL the tracking channels receive PVT feedback information from the navigator. Moreover, a PCRLB-based performance evaluation with

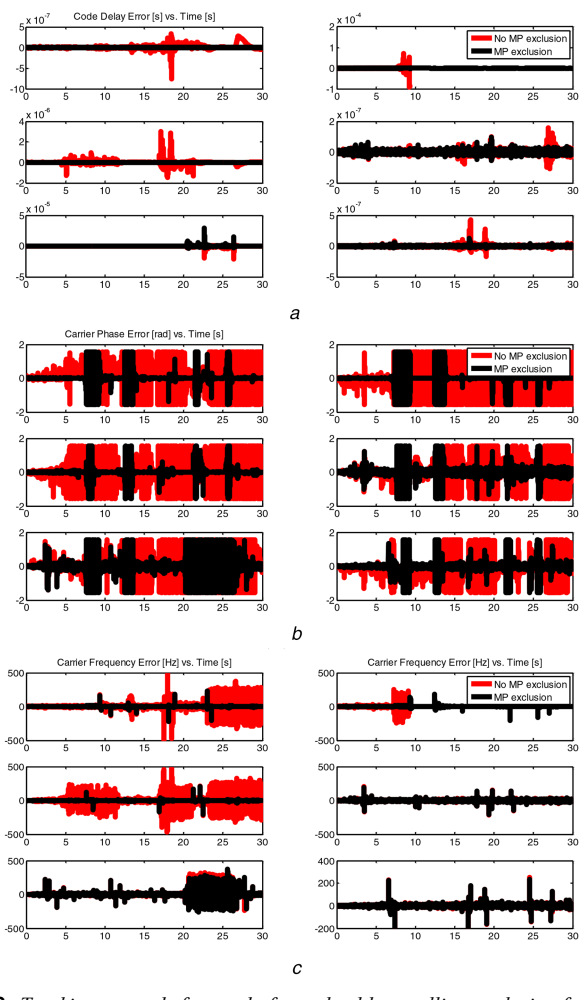


Fig. 8 Tracking errors before and after unhealthy satellites exclusion from PVT (top to bottom, left to right: PRN05, PRN15, PRN27, PRN07, PRN09, PRN26; constellation 1, scenario 1)
(a) Code delay errors, (b) Carrier phase errors, (c) Carrier frequency errors

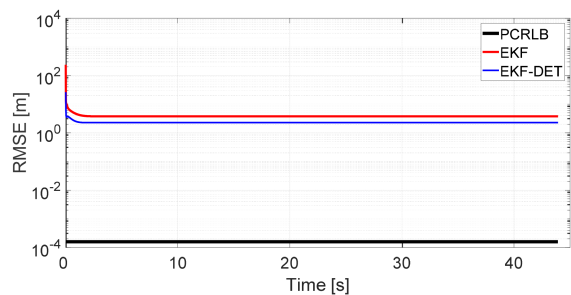


Fig. 9 PCRLB-based performance evaluation, EKF, EKF-DET, and PCRLB. Scenario 3

Monte Carlo simulations shows that the proposed MP detector improves the EKF RMSE performance. Also, the detection test can be applied with minor adjustments to other GNSSs such as Galileo, GLONASS, and Compass.

9 Acknowledgments

The authors would like to thank the French Space Agency (CNES) and the French South African Institute of Technology (FSATI) for the financial support to this research.

10 References

[1] Mubarak, O., Dempster, A.: 'Exclusion of multipath-affected satellites using early late phase', *J. Global Positioning Syst.*, 2010, **9**, (2), pp. 145–155
[2] Mubarak, O.: 'Analysis of early late phase for multipath mitigation'. ION GNSS 21st Int. Technical Meeting of the Satellite Division, Savannah, GA, USA, 16–19 September 2008, pp. 669–678

[3] Brennehan, M., Morton, Y., Zhou, Q.: 'An ANOVA-based GPS multipath detection algorithm using multi-channel software receivers'. Proc. 2008 IEEE/ION Position, Location and Navigation Symp., Monterey, CA, USA, 2008
[4] Brennehan, M.T., Morton, Y.T., Zhou, Q.: 'GPS multipath detection with ANOVA for adaptive arrays', *IEEE Trans. Aerosp. Electron. Syst.*, 2010, **46**, (3), pp. 1171–1184
[5] Pinana-Diaz, C., Toledo-Moreo, R., Betaille, D., et al.: 'GPS multipath detection and exclusion with elevation-enhanced maps'. Proc. 2011 14th Int. IEEE Conf. on Intelligent Transportation Systems, Washington, DC, USA, 5–7 October 2011
[6] Lee, H.K., Lee, J.G., Jee, G.-I.: 'GPS multipath detection based on sequence of successive-time double-differences', *IEEE Signal Process. Lett.*, 2004, **11**, (3), pp. 316–319
[7] Fang, Y., Hong, Y., Zhou, O., et al.: 'A GNSS satellite selection method based on SNR fluctuation in multipath environments', *Int. J. Control Autom.*, 2015, **8**, (11), pp. 313–324
[8] Lopez-Salcedo, J.A., Parro-Jimenez, J.M., Seco-Granados, G.: 'Multipath detection metrics and attenuation analysis using a GPS snapshot receiver in harsh environments'. 2009 3rd European Conf. on Antennas and Propagation, Berlin, 2009
[9] Beitler, A., Tollkuehn, A., Giustiniano, D., et al.: 'CMCD: multipath detection for mobile GNSS receivers'. Proc. of 2015 Int. Technical Meeting of the Institute of Navigation, Dana Point, California, 26–28 January 2015
[10] Egea-Roca, D., Seco-Granados, G., López-Salcedo, J.A., et al.: 'Signal-level integrity and metrics based on the application of quickest detection theory to multipath detection'. Proc. 28th Int. Technical Meeting of the Satellite Division of the Institute of Navigation (ION GNSS+2015), Tampa, Florida, 14–18 September 2015
[11] Dierendonck, A., Fenton, P., Ford, T.: 'Theory and performance of narrow correlator spacing in a GPS receiver', *Navig., J. Inst. Navig.*, 1992, **39**, (3), pp. 265–283
[12] Veitsel, V., Zhdanov, A., Zhodzichsky, M.: 'The mitigation of multipath errors by strobe correlators in GPS/GLONASS receiver', *GPS Solut.*, 1998, **2**, (2), pp. 38–45
[13] McGraw, G.: 'Practical GPS carrier phase multipath mitigation using high resolution correlator techniques'. Proc. IAIN World Congress/ION Annual Meeting, San Diego, CA, USA, 2000, pp. 373–381
[14] McGraw, G., Braasch, M.: 'GNSS multipath mitigation using gated and high resolution correlator concepts'. Proc. ION National Technical Meeting, San Diego, CA, USA, 1999, pp. 333–342
[15] Townsend, B., Fenton, P.: 'A practical approach to the reduction of pseudorange multipath errors in a L1 GPS receiver'. Proc. 7th Int. Technical Meeting of the Satellite Division of the Institute of Navigation, Part 1 (of 2), Proc. ION GPS, Salt Lake City, UT, USA, 1994, vol. 1, pp. 143–148
[16] Sleewaegen, J., Boon, F.: 'Mitigating short-delay multipath: a promising new technique'. Proc. ION GPS, Salt Lake City, UT, USA, 11–14 September 2001, pp. 204–213
[17] Closas, P., Carles, F.-P., Diez, J., et al.: 'Nonlinear Bayesian tracking loops for multipath mitigation', *Int. J. Navig. Obs.*, 2012, **2012**, pp. 1–15, no. Article ID 359128
[18] van Nee, R.: 'The multipath estimating delay lock loop'. IEEE 2nd Int. Symp. on Spread Spectrum Techniques and Applications, Yokohama, Japan, 1992, pp. 39–42
[19] Cahn, C., Chansarkar, M.: 'Multipath corrections for a GPS receiver'. Proc. 10th Int. Technical Meeting of the Satellite Division of the Institute of Navigation (ION-GPS), Kansas City, MO, USA, 1997, vol. 1, pp. 551–557
[20] Weil, L.: 'Multipath mitigation using modernized GPS signals: how good can it get?'. Proc. 17th Int. Technical Meeting of the Satellite Division of the Institute of Navigation (ION GPS), Long Beach, CA, USA, 2002, pp. 493–505
[21] Fenton, P., Jones, J.: 'The theory and performance of NovAtel Inc.'s vision correlator'. Proc. 19th Int. Technical Meeting of the Satellite Division of the Institute of Navigation (ION GNSS'05), Fort Worth, TX, USA, September 2005, pp. 2178–2186
[22] Sahnoudi, M., Landry, R.: 'Multipath mitigation techniques using maximum-likelihood principle'. *Inside GNSS*, 2008, **3**, (8), pp. 24–29
[23] Sahnoudi, M., Amin, M.G.: 'Fast iterative maximum-likelihood algorithm (FIMLA) for multipath mitigation in the next generation of GNSS receivers', *IEEE Trans. Wirel. Commun.*, 2008, **7**, (11), pp. 4362–4374
[24] Kumar, D., Lau, K.: 'Deconvolution approach to carrier and code multipath error elimination in high precision GPS'. Proc. 1996 National Technical Meeting of the Institute of Navigation, Santa Monica, CA, USA, January 1996, pp. 729–737
[25] Lohan, S., Skournetou, D., Sayed, A.: 'A deconvolution algorithm for estimating jointly the line-of-sight code delay and carrier phase of GNSS signals'. ENC-GNSS, Naples, Italy, 2009
[26] Yang, C., Porter, L.: 'Frequency-domain characterization of GPS multipath for estimation and mitigation'. Proc. 18th Int. Technical Meeting of the Satellite Division of the Institute of Navigation (ION-GNSS), Long Beach, CA, USA, September 2005
[27] Yang, C., Porter, L.: 'Multipath-desensitized delay estimation with GPS signal channel transfer function filtering'. ION 61st Annual Meeting, Cambridge, MA, USA, June 2005
[28] Amani, E., Djouani, K., Kurien, A., et al.: 'GPS multipath detection in the frequency domain'. European Navigation Conf. (ENC), Helsinki, 2016
[29] Brown, R.: 'Receiver autonomous integrity monitoring', in Parkinson, B.W., Spilker, J.J.Jr. (Eds.): 'Global positioning system: theory and applications', vol. 2 (IAA, Inc., Washington, D.C., 1996), pp. 143–165
[30] Groves, P.: 'Fault detection and integrity monitoring' in 'Principles of GNSS, inertial, and multisensor integrated navigation systems' (Artech House, Boston, London 2008), pp. 451–470

[31] Clark, B.: 'Fault detection and exclusion in deeply integrated GPS/INS navigation'. PhD thesis, Auburn University, Auburn, Alabama, 2012

[32] Giremus, A., Tourneret, J.-Y., Calmettes, V.: 'A particle filtering approach for joint detection/estimation of multipath effects on GPS measurements', *IEEE Trans. Signal Process.*, 2007, **5**, (4), pp. 1275–1285

[33] Viandier, N., Nahimana, D., Marais, J., et al.: 'GNSS performance enhancement in urban environment based on pseudo-range error model'. Proc. IEEE/ION PLANS, Monterey, 2008

[34] Spangenberg, M., Calmettes, V., Julien, O., et al.: 'Detection of variance changes and mean value jumps in measurement noise for multipath mitigation in urban navigation', *J. Inst. Navig.*, 2010, **57**, (1), pp. 35–52

[35] Ray, J.: 'Mitigation of GPS code and carrier phase multipath effects using a multi-antenna system'. PhD thesis, March 2000

[36] Heiries, V.: 'Optimisation d'une chaîne de réception pour signaux de radionavigation par satellite à porteuse à double décalage (BOC)'. PhD thesis, 2007

[37] Kay, S.: 'Fundamentals of statistical signal processing, volume II: detection theory' (Prentice Hall, New Jersey, USA, 1998)

[38] Chan, Y., Yuan, Q., So, H., et al.: 'Detection of stochastic signals in the frequency domain', *IEEE Trans. Aerosp. Electron. Syst.*, 2001, **37**, (3), pp. 978–988

[39] Falletti, E., Pini, M., Lo Presti, L.: 'Low complexity carrier-to-noise ratio estimators for GNSS digital receivers', *IEEE Trans. Aerosp. Electron. Syst.*, 2011, **47**, (1), pp. 420–437

[40] Kay, S.: 'Fundamentals of statistical signal processing volume I: estimation theory' (Prentice Hall, New Jersey, USA, 1993)

11 Appendices

11.1 Appendix 1: derivation of MP detector metric

The Neyman–Pearson theorem [37] states that for a binary hypothesis test between two hypotheses H_0 and H_1 , to maximise the PD given a PFA = α , H_1 is chosen if

$$L(x) = \frac{p(x; H_1)}{p(x; H_0)} > T. \quad (16)$$

The threshold T is derived from $PFA = \int_{\{x: L(x) > T\}} p(x; H_0) dx = \alpha$. The function $L(x)$ is called the likelihood ratio. It indicates for each value of x the likelihood of H_1 versus the likelihood of H_0 . The test of (16) is called the likelihood ratio test.

The proposed FFT-based MP detector metric can be derived by considering that the EmL correlator output is a sinusoid, which is the case in general. Given the following sinusoidal detection problem:

$$\begin{aligned} H_0: x[n] &= w[n], \\ H_1: x[n] &= A \cos(2\pi f_0 n + \phi) + w[n], \quad \text{with } n \in \{0, 1, \dots, N-1\} \end{aligned}$$

where $w[n]$ is white Gaussian noise with known variance σ^2 , for unknown amplitude A , phase ϕ , and frequency f_0 , the generalised likelihood ratio test (GLRT) decides H_1 if

$$\begin{aligned} \frac{p(x; \hat{A}, \hat{\phi}, \hat{f}_0, H_1)}{p(x; H_0)} &> T \text{ or } \frac{\max_{f_0} p(x; \hat{A}, \hat{\phi}, f_0, H_1)}{p(x; H_0)} > T, \\ \therefore \max_{f_0} \frac{p(x; \hat{A}, \hat{\phi}, f_0, H_1)}{p(x; H_0)} &> T, \\ \therefore \ln \max_{f_0} \frac{p(x; \hat{A}, \hat{\phi}, f_0, H_1)}{p(x; H_0)} &> \ln T, \\ \therefore \max_{f_0} \ln \frac{p(x; \hat{A}, \hat{\phi}, f_0, H_1)}{p(x; H_0)} &> \ln T. \end{aligned} \quad (17)$$

Let $Y(x) = p(x; \hat{A}, \hat{\phi}, \hat{f}_0, H_1)/p(x; H_0)$ be the generalised likelihood ratio. For a random value of f_0 that is known, $Y(x) = p(x; \hat{A}, \hat{\phi}, H_1)/p(x; H_0)$ (see equation below). It is shown in [40] that the MLE of $Y(x)$ for large N is approximately

$$\hat{A} = \sqrt{\hat{\beta}_1^2 + \hat{\beta}_2^2} \quad \text{and} \quad \hat{\phi} = \tan^{-1} \left(\frac{-\hat{\beta}_2}{\hat{\beta}_1} \right), \quad (18)$$

where $\hat{\beta}_1 = (2/N) \sum_{n=0}^{N-1} x[n] \cos 2\pi f_0 n$ and $\hat{\beta}_2 = (2/N) \sum_{n=0}^{N-1} x[n] \sin 2\pi f_0 n$. Furthermore

$$\begin{aligned} \ln Y(x) &= \ln \left[\exp \left[-\frac{1}{2\sigma^2} \sum_{n=0}^{N-1} (x[n] - \hat{A} \cos(2\pi f_0 n + \hat{\phi}))^2 \right] \right] \\ &\quad - \ln \left[\exp \left[-\frac{1}{2\sigma^2} \sum_{n=0}^{N-1} x^2[n] \right] \right], \end{aligned}$$

(see equation below). However

$$\begin{aligned} \sum_{n=0}^{N-1} x[n] \hat{A} \cos(2\pi f_0 n + \hat{\phi}) &= \sum_{n=0}^{N-1} x[n] \cos(2\pi f_0 n) \hat{A} \cos \hat{\phi} \\ &\quad - \sum_{n=0}^{N-1} x[n] \sin(2\pi f_0 n) \hat{A} \sin \hat{\phi}. \end{aligned}$$

Also, $\cos(\tan^{-1}(\theta)) = 1/\sqrt{1+\theta^2}$ and $\sin(\tan^{-1}(\theta)) = \theta/\sqrt{1+\theta^2}$. By using (18), $\hat{A} \cos \hat{\phi} = \hat{\beta}_1$ and $-\hat{A} \sin \hat{\phi} = \hat{\beta}_2$. Thus

$$\sum_{n=0}^{N-1} x[n] \hat{A} \cos(2\pi f_0 n + \hat{\phi}) = \frac{N}{2} (\hat{\beta}_1^2 + \hat{\beta}_2^2). \quad (19)$$

Moreover, by using the formula of the power of a sinusoidal signal, $\sum_{n=0}^{N-1} \cos^2(2\pi f_0 n + \hat{\phi})$ can be evaluated. The power of a periodic sinusoid $x[n] = A \cos(2\pi f_0 n + \hat{\phi})$ is given by $P_N = (1/N) \sum_{n=0}^{N-1} A^2 \cos^2(2\pi f_0 n + \hat{\phi})$.

Furthermore, Euler's formula establishes that

$$\cos(2\pi f_0 n + \hat{\phi}) = \frac{1}{2} \left[e^{j(2\pi f_0 n + \hat{\phi})} + e^{-j(2\pi f_0 n + \hat{\phi})} \right].$$

$$Y(x) = \frac{(1/(2\sigma^2)^{N/2}) \exp \left[-(1/2\sigma^2) \sum_{n=0}^{N-1} (x[n] - \hat{A} \cos(2\pi f_0 n + \hat{\phi}))^2 \right]}{(1/(2\sigma^2)^{N/2}) \exp \left[-(1/2\sigma^2) \sum_{n=0}^{N-1} x^2[n] \right]}.$$

$$\ln Y(x) = \left[-\frac{1}{2\sigma^2} \sum_{n=0}^{N-1} (x[n] - \hat{A} \cos(2\pi f_0 n + \hat{\phi}))^2 \right] + \left[\frac{1}{2\sigma^2} \sum_{n=0}^{N-1} x^2[n] \right],$$

$$\ln Y(x) = -\frac{1}{2\sigma^2} \left[\sum_{n=0}^{N-1} -2x[n] \hat{A} \cos(2\pi f_0 n + \hat{\phi}) + \sum_{n=0}^{N-1} \hat{A}^2 \cos^2(2\pi f_0 n + \hat{\phi}) \right].$$

For a bin frequency, $2\pi f_0 = 2\pi(m/N)$, $m = 1, 2, \dots, N-1$.
Therefore

$$\begin{aligned} P_N &= \frac{1}{N} \sum_{n=0}^{N-1} A^2 \cos^2(2\pi f_0 n + \hat{\phi}), \\ P_N &= \frac{A^2}{4N} \sum_{n=0}^{N-1} \left(e^{j(2\pi f_0 n + \hat{\phi})} + e^{-j(2\pi f_0 n + \hat{\phi})} \right)^2, \\ P_N &= \frac{A^2}{4N} \left(\sum_{n=0}^{N-1} e^{2j(2\pi f_0 n + \hat{\phi})} \right) + \frac{A^2}{4N} \left(\sum_{n=0}^{N-1} e^{-2j(2\pi f_0 n + \hat{\phi})} \right) \\ &\quad + \frac{A^2}{4N} 2N, \end{aligned}$$

because for $\Omega_0 = 2\pi f_0 = 0$, $x[n] = A \cos \hat{\phi}$ with $N = 1$.
Therefore

$$P_N = \frac{A^2}{2} + e^{2j\hat{\phi}} S_1 + e^{-2j\hat{\phi}} S_2 = \frac{A^2}{2},$$

where

$$\begin{aligned} S_1 &= \sum_{n=0}^{N-1} e^{2j(2\pi f_0 n)} = \sum_{n=0}^{N-1} e^{2j(2\pi(m/N)n)}. \quad \text{Let } z_1 = e^{2j(2\pi(m/N))} \\ \therefore S_1 &= \sum_{n=0}^{N-1} z_1^n = \frac{z_1^N - 1}{z_1 - 1} = 0 \quad \text{because } z_1^N = 1. \\ S_2 &= \sum_{n=0}^{N-1} e^{-2j(2\pi f_0 n)} = \sum_{n=0}^{N-1} e^{-2j(2\pi(m/N)n)}. \quad \text{Let } z_2 \\ &= e^{-2j(2\pi(m/N))}, \\ \therefore S_2 &= \sum_{n=0}^{N-1} z_2^n = \frac{z_2^N - 1}{z_2 - 1} = 0 \quad \text{because } z_2^N = 1. \end{aligned}$$

In summary, for large N (i.e. $N > 2$), the power of the periodic sinusoid $x[n] = A \cos(2\pi f_0 n + \hat{\phi}) = A \cos(2\pi(m/N)n + \hat{\phi})$ is given by $P_N = (1/N) \sum_{n=0}^{N-1} A^2 \cos^2(2\pi f_0 n + \hat{\phi}) = A^2/2$. For $A = 1$, we have $x[n] = \cos(2\pi f_0 n + \hat{\phi})$ and $P_N = (1/N) \sum_{n=0}^{N-1} \cos^2(2\pi f_0 n + \hat{\phi}) = 1/2$. Therefore

$$\sum_{n=0}^{N-1} \cos^2(2\pi f_0 n + \hat{\phi}) = \frac{N}{2}. \quad (20)$$

Substitution of (19) and (20) into $\ln Y(x)$ yields

$$\begin{aligned} \ln Y(x) &= -\frac{1}{2\sigma^2} \left[\sum_{n=0}^{N-1} -2\frac{N}{2} (\hat{\beta}_1^2 + \hat{\beta}_2^2) + \frac{N}{2} \hat{A}^2 \right] \\ &= \frac{N}{4\sigma^2} (\hat{\beta}_1^2 + \hat{\beta}_2^2). \end{aligned}$$

However

$$\begin{aligned} \hat{\beta}_1^2 + \hat{\beta}_2^2 &= \left(\frac{2}{N} \right)^2 \left[\left(\sum_{n=0}^{N-1} x[n] \cos 2\pi f_0 n \right)^2 + \left(\sum_{n=0}^{N-1} x[n] \sin 2\pi f_0 n \right)^2 \right], \\ \hat{\beta}_1^2 + \hat{\beta}_2^2 &= \frac{4}{N} \frac{1}{N} \left| \sum_{n=0}^{N-1} x[n] \exp(-j2\pi f_0 n) \right|^2 = \frac{4}{N} \Omega(f_0). \end{aligned}$$

Therefore, $\ln Y(x) = (N/4\sigma^2)(4/N)\Omega(f_0)$

$$\ln Y(x) = \frac{1}{\sigma^2} \Omega(f_0) \quad (21)$$

where $\Omega(f_0)$ is the periodogram evaluated at $f=f_0$. Thus, the GLRT decides H_1 if $\max_{f_0} \ln Y(x) > \ln T \therefore \max_{f_0} (\Omega(f_0)/\sigma^2) > \ln T$. Let $\eta = \ln T$ be the threshold and the FFT-based detection test proposed in this paper is obtained as follows:

$$\max_{f_0} \frac{\Omega(f_0)}{\sigma^2} \underset{H_1}{>} \eta \quad \text{or} \quad \max_{f_0} \frac{\Omega(f_0)}{\sigma^2} \underset{H_0}{<} \eta. \quad (22)$$

11.2 Appendix 2: derivation of MP detector threshold

For a problem of detection of a signal in white Gaussian noise formulated by a GLRT that has been reduced to

$$N \ln \left[1 + \frac{P}{\sigma^2} \right] \underset{H_1}{>} \gamma \quad \text{or} \quad N \ln \left[1 + \frac{P}{\sigma^2} \right] \underset{H_0}{<} \gamma, \quad (23)$$

with N being the size of the samples considered in the test, P the maximum or average signal power estimation metric, and σ^2 the MLE of noise variance, the detection threshold is given by [37]

$$\gamma = \left[\text{cdf}^{-1} \left(1 - \frac{\text{PFA}}{2} \right) \right]^2, \quad (24)$$

where cdf is the cumulative distribution function of the standard normal distribution, cdf^{-1} the inverse cumulative distribution function, and the PFA. Equation (23) can be rewritten as

$$\frac{P}{\sigma^2} \underset{H_1}{>} \exp\left(\frac{\gamma}{N}\right) - 1 \quad \text{or} \quad \frac{P}{\sigma^2} \underset{H_0}{<} \exp\left(\frac{\gamma}{N}\right) - 1. \quad (25)$$

Equation (25) is similar to the defined MP detector metric with the detection threshold being as follows:

$$\eta = \exp \left\{ \frac{[\text{cdf}^{-1}(1 - \text{PFA}/2)]^2}{N} \right\} - 1. \quad (26)$$